U.PORTO

FEUP FACULDADE DE ENGENHARIA UNIVERSIDADE DO PORTO

MESTRADO INTEGRADO EM ENGENHARIA DO AMBIENTE

2016/2017

HYDROGEN PRODUCTION FROM WATER GAS SHIFT REACTION IN A PD-AG MEMBRANE REACTOR WITH A CU-BASED CATALYST

CÁTIA SOFIA DAS DORES ESPIRITO SANTO

Dissertação submetida para obtenção do grau de

MESTRE EM ENGENHARIA DO AMBIENTE

Presidente do Júri: Cidália Maria de Sousa Botelho
(Professora Auxiliar do Departamento de Engenharia Química da Faculdade de Engenharia da Universidade do Porto)

_____

Orientador académico: Luís Miguel Madeira
(Professor Associado do Departamento de Engenharia Química da Faculdade de Engenharia da Universidade do Porto)

Orientador na empresa: Alessia Santucci
(Researcher at the ENEA Frascati Research Center, Department of Fusion Technology - Membrane Laboratory)

“(...) Hydrogen is not as far away as we think it is.”

- *Bob Inglis*

Acknowledgements:

In my life, a Master thesis does not only represent the end of a cycle of studies. That is probably the last thing it stands for. This master thesis represents another accomplished goal in my life that I fought really hard to achieve. In a life with a lot of struggle, university was always a question mark, so being able to deliver this master thesis means more than words could ever tell.

Evidently, this wouldn't be possible without the support of the strongest pillar in my life: my Mother. Mother and father, she taught me how to fight for what I wanted and do whatever it took to get it with humbleness and it is because of her and her personal fights that I can do all of this; finish my master degree in environmental engineering and my Master thesis in Italy. It was never easy, but we made it. And are not enough "*thank yous*". Not only for all the opportunities that she gave me never asking for anything in return but my smile through life but also for the person she inspired me to be. That is something I will never be able to repay an I will be forever thankful to her.

Also, I would like to thank my brothers -Rui and David -, my stepfathers Nuno e João, my grandmas and grandma-aunt Paz, my aunt Alexandra and uncle João and my cousins, because they were my biggest fans through all this journey.

Another person I'd like to thank is Sofia Crudo for being my right hand in Italy. For helping me get through it since I step foot in the airport, for letting me stay with her until I found a room of my own and everything she done for me since. It is the kind of generosity one will never be able to repay.

I would like to thank also all the ENEA family. Alessia and Marco that worked closely to me every day, helping me unconditionally every single time I needed it, for all the knowledge I could absorb from them both, but not only; I must thank them specially for the kindness and the friendship they showed me, the limitless patience they had. So, thank you very, *very* much. Thank you, Marco Ecclesia, for all the knowledge you shared with me in the first weeks of experiments and all the good time we had together in the laboratory. It was really good to have you as my partner. Thank you, Giullia and Eleonora for being the best office partners and the best translators one could ever get. Thank you "Neutronic people", especially Andrea for all the friendship. Thank you, Sara Rispoli, for being the sweetest person I've ever met. Thank you, Giacomo, for sharing the GC with me and the laughs while waiting for the results. Thank you, Raffaele and Fabio, for making my lunch time much funnier. Thank you, Silvano, for all the nice words and encouragement when I needed it.

Thank you, professor Luis Miguel Madeira, for the patience he had during this time. It wasn't easy and I'm really grateful for all the time you spent to help me. Not only about the thesis but everything else. Thank you very much.

And, of course, thank you to everyone that contributed one way or another for everything that I am today. My best friend since I was 8, Catarina Almeida, especially.

Abstract:

As a student of the Faculty of Engineering of the University of Porto, the period between August and January (lasting 5 months) was spent working in the ENEA Frascati laboratories (Rome, Italy) to perform work in the field of hydrogen production/purification for the master thesis in Environmental Engineering, supported by the ERASMUS program. It has been tested the hydrogen permeation and production via water gas shift reaction in a membrane reactor with a new catalyst (copper-based catalyst), under a set of experimental conditions. The measured performances were compared with results of other catalysts previously tested at ENEA.

Therefore, this work has the goal of analysing the permeation of a Pd-based membrane towards hydrogen and, also, the performance of such membrane in the water gas shift (WGS, $CO + H_2O \rightleftharpoons CO_2 + H_2$) reaction making use of a membrane reactor with the new catalyst; it was in short aimed to evaluate the efficiency, in terms of hydrogen yield, in a membrane reactor device. This was studied in a membrane made of a 142.9 µm thick Pd-Ag (25 wt.% of Ag) tube filled with 16 g of a commercial copper-based catalyst (HiFuel ®).

The studies were performed at different pressures (2 bar, 3 bar, 4 bar and 5 bar) and temperatures (250 °C, 300 °C and 350 °C). With regard to the permeation tests, they were carried out by using different H_2/He feed molar ratios. In this way, an experimental trend of the hydrogen permeating flow vs. hydrogen partial pressure across the membrane has been assessed, which obeys the Sieverts' law.

The catalyst tested in the WGS reaction showed to have a good performance when it came to CO conversion and therefore there was a high production of hydrogen and CO2. Also, this system has proven to produce low amount of CH4, only starting to produce such species at higher temperatures (300 and 350 °C). When compared to other catalysts tested at ENEA, the Cu-based material showed a lower efficiency but a better result on what concerns low selectivity towards sub-products such as methane. However, more tests should be made in the future in order to test the catalyst stability and the reproducibility of the results obtained.

Declaração:

Declara, sob compromisso de honra, que este trabalho é original e que todas as contribuições não originais foram devidamente referenciadas com identificação da fonte.

LIST OF CONTENTS

1 Hydrogen Production and Separation 1

2 Membrane Separation 3

2.1 Metallic Membranes 4

2.1.1 Palladium based membranes 6

3 Water Gas Shift Reaction 9

3.1 Catalyst 9

4 Experimental Setup 11

5 Permeation tests 13

5.1 Conditions 14

5.2 Results and Discussion 15

6 Water Gas Shift: Reaction tests 20

6.1 Catalyst 20

6.2 Water Gas Shift Conditions 21

6.3 Water Gas Shift: Results and Discussion 22

6.3.1 Influence of the temperature 22

6.3.2 Catalyst cycling 25

6.4 Water Gas Shift: Different catalysts 29

6.4.1 Results comparison among different catalysts 30

7 Conclusions 33

8 References 34

9 Appendix 36

A. Sieverts' law graphics with flux of hydrogen permeated vs. driving force 36

B. Experimental Procedure of the Permeation and Reaction Tests 38

Starting procedure: 38

Cool down procedure: 38

Leak test procedure: 38

C. Calibration Curves used in the GC during the Reaction Tests 40

FIGURES CAPTIONS

Figure 2.1 - Schematic representation of two phase process separated with a membrane. . 3
Figure 2.2- Schematic representation of a membrane process where the feed was separated into retentate and permeate. 3
Figure 2.3 - Scheme of the solution-diffusion mechanism in a dense metallic membrane (Nenoff, 2007) 5
Figure 2.4 - P-C-T phase diagram of the palladium hydrogen system (Yun, 2011). 7
Figure 2.5 - Relative performance of the various H2 membrane materials (McLeod, 2008). 7
Figure 2.6 - The influence of alloy composition on the pure hydrogen permeability for Pd-alloy membranes containing Au, Cu and Ag at 350°C (Hatlevik, 2010). 8
Figure 4.1 - Experimental Plant of the Reactor (Autor: Incelli, M. 2016). 11
Figure 5.1 - Measured permeability at different pressure conditions for He/H_2=1 (feed ratio). 15
Figure 5.2 – Permeation efficiency for each lumen pressure and temperature tested at H_2/He=8. 17
Figure 5.3 - Permeation efficiency for each lumen pressure and temperature tested at H_2/He=1. 17
Figure 5.4 - Permeation efficiency for each lumen pressure and temperature tested at H_2/He=0.125. 18
Figure 5.5 - Hydrogen permeation efficiency per the driving force (ΔP) at each tested temperature 18
Figure 6.1 – Efficiency of the system at the temperatures of 250, 300 and 350 °C, at different lumen pressures 22
Figure 6.2 – Dioxide Carbon percentage in the retentate side using WSGR at a temperature of 250°C, 300°C and 350°C 23
Figure 6.3 – Hydrogen percentage in the retentate side using WSGR at a temperature of 250°C, 300°C and 350°C 24
Figure 6.4 – Methane percentage in the retentate side using WSGR at a temperature of 250°C, 300°C and 350°C 24
Figure 6.5 -Efficiency at 300°C before the permeation test (Normal) and after the permeation test going up from 2 to 5 bar (Up) and down from 5 to 2 bar (Down). 26
Figure 6.6 – Carbon dioxide percentage in the retentate side using WSGR at a temperature of 300°C (before the permeation test) and varying the pressure from 2 to 5 bar (300°C Up) and reversed (300°C Down) 26

Figure 6.7 – Hydrogen percentage in the retentate side using WSGR at a temperature of 300°C (before the permeation test) and varying the pressure from 2 to 5 bar (300°C Up) and reversed (300°C Down). 27

Figure 6.8 – Methane percentage in the retentate side using WSGR at a temperature of 300°C (before the permeation test) and varying the temperature from 2 to 5 bar (300°C Up) and reversed (300°C Down)..... 28

Figure 6.9 - Efficiency of the system using three different catalysts [Cat 1 – Non-commercial Platinum and silica; Cat 2 – Commercial catalyst (BASF) Platinum based with alumina support; Cat 3 – Cu based commercial catalyst (tested in this work).] 30

Figure 6.10 – CH_4 in the retentate side from WSGR using three different catalysts [Cat 1 – Non-commercial Platinum and silica; Cat 2 – Commercial catalyst (BASF) Platinum based with alumina support and Cat 3 – Cu based commercial catalyst (tested in this work).]..... 31

Figure 6.11 – CO_2 in the retentate side from WSGR using three different catalysts [Cat 1 – Non-commercial Platinum and silica; Cat 2 – Commercial catalyst (BASF) Platinum based with alumina support; Cat 3 – Cu based commercial catalyst (tested in this work).] 31

Figure 9.1 - Permeated flux of hydrogen [mol m^{-2} s^{-1}] as a function of the applied driving force [$Pa^{0.5}$] at a temperature of 400 °C 36

Figure 9.2 - Permeated flux of hydrogen [mol m^{-2} s^{-1}] as a function of the applied driving force [$Pa^{0.5}$] at a temperature of 350 °C 36

Figure 9.3 - Permeated flux of hydrogen [mol m^{-2} s^{-1}] as a function of the applied driving force [$Pa^{0.5}$] at a temperature of 300 °C 37

Figure 9.4 - Permeated flux of hydrogen [mol m-2 s-1] as a function of the applied driving force [$Pa^{0.5}$] at a temperature of 250 °C..... 37

Figure 9.5 – Calibration Curve of the Gas Chromatograph for CO_2..... 40

Figure 9.6 - Calibration Curve of the Gas Chromatograph for H_2 40

Figure 9.7 - Calibration Curve of the Gas Chromatograph for CH_4..... 41

TABLES CAPTIONS

Table 5.1 - Operational conditions for the permeation tests (flow rates and ratios) 14

Table 5.2 – Experimental conditions inside the reactor (Membrane temperature and Lumen pressure) 14

Table 5.5 - Published results of Pre-exponential factor and activation energy 16

Table 6.1 - Catalyst activation conditions 21

Table 6.2 – Reaction test conditions 21

Table 6.3 - Results of the permeation tests before and after the reaction test. 25

Table 6.4 - Shell pressure in all the tests at 2 bar lumen pressure 27

Table 6.5 – Catalyst properties 29

NOTATION AND GLOSSARY

LIST OF ACRONYMS

ENEA	Italian National Agency for New Technologies, Energy and Sustainable Economic Development
GC	Gas Chromatograph
LFC	Liquid Flow Controller
MFC	Mass Flow Controller
MR	Membrane Reactor
sccm	Standard cubic centimetre per minute
WGS	Water Gas Shift
WGSR	Water Gas Shift Reaction

SYMBOLS

$\propto$	Selectivity factor
A	Area of permeation (m^2)
C	Hydrogen Concentration (mol^{-3})
D	Diffusion coefficient ($m^2\ s^{-1}$)
E_a	Activation energy for the permeation ($J\ mol^{-1}$)
F_i	Feed flow rate of specie *i* ($mol\ s^{-1}$)
J_{H_2}	Diffusional flux of hydrogen ($mol^{-2}\ s^{-1}$)
P_{H2O}	Partial pressure of hydrogen (Pa)
P	Pressure (Pa)
Pe	Hydrogen permeability ($mol\ m^{-1}\ s^{-1}\ Pa^{-0.5}$)
S	Solubility coefficient ($mol\ m^{-3}\ Pa^{-0.5}$)
T	Temperature (K)
t	Thickness (µm)
V	Volume (m^3)

CONSTANTS

R = 8.314 J mol-1 K-1

1 HYDROGEN PRODUCTION AND SEPARATION

In an era of Environmental awareness, the world is doing whatever it can to reduce and/or limit global average temperature but, for it to happen, there is a need to develop alternative energy sources. Among renewable/clean energies, hydrogen emerges to play an important role in the future energy mix. Some researchers even have shown that the useful energy output per quantity of natural fuel can be doubled by producing hydrogen from natural fuels and using that hydrogen in fuel cells to power electric motors (Witjens, 2004).

The cost of hydrogen, though, is high enough for it not to be considered an economically viable option. For that reason, there is a need to implement new processes that would reduce the equipment needed to generate and purify hydrogen.

Hydrogen can be produced from widely available primary energy sources including fossil fuels and renewables, which means it can be considered as a very promising energy vector. These days, hydrogen production technologies fall into three general categories: thermal, electrolytic and photolytic processes. Yet, the problem with catalytic reaction technologies to convert natural gas, coal, biomass and a few other components into a H_2-rich stream is that, along with it, it is also produced small amounts of impurities (e.g. CO, CH_4), which will demand a purification process that includes one of the following procedures: pressure swing adsorption (PSA), cryogenic distillation or membrane separation.

Particularly, membrane separation is currently considered to be more and more promising because of low energy consumption, for the possibility of continuous and easy operation, and finally for its cost-effectiveness relation. Particularly, the integration of Pd-Ag membranes into water gas shift (WSG) reactors provides a new effective solution, because it produces a high-purity hydrogen stream and allows overcoming the equilibrium limitations of such reversible reaction experienced in conventional reactor configurations.

Considering these aspects, this work has the aim of investigating the production of highly pure hydrogen through the water gas shift reaction in a Pd-Ag membrane reactor. This membrane reactor was made of thin walled Pd-Ag with 25 wt % Ag, filled with a commercial copper-based catalyst. Moreover, these tests were performed by varying the conditions of the system, such as membrane temperature and the lumen pressure. The results obtained about the efficiency of the system with the Cu-based catalyst were furthermore compared with other results obtained with

other catalysts, tested prior to this work, at *Frascati Research Centre of ENEA (Italian National Agency for New Technologies and Sustainable Economic Development).*

The first step was to perform some permeation tests to determine the properties of the Pd-Ag membrane to be used in the reaction tests.

2 MEMBRANE SEPARATION

A membrane is a barrier that allows a selective mass transportation between two phases. It is considered selective because some components may pass through these barriers while others may not. This singularity makes membranes suitable to separate a mixture of components. This kind of permeation is attained by applying a driving force through the membrane that can be in the form of pressure difference, temperature, concentration or electrical potential gradient. A schematic illustrating the selective transport and separation across a membrane can be observed in figure 2.1.

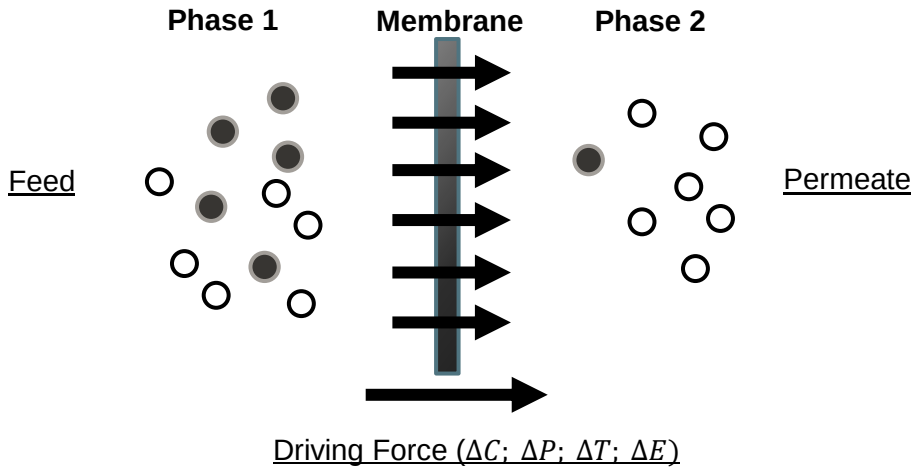

Figure 2.1 - Schematic representation of two phase process separated with a membrane.

Membrane technologies are very interesting nowadays, when it comes to the separation of molecular mixtures because of their continuous operation and because, such separation, occurs only by physical processes, meaning the components remain chemically unaltered. In these processes, there are two different streams obtained from the main stream, the retentate and the permeate side, as illustrated in figure 2.2.

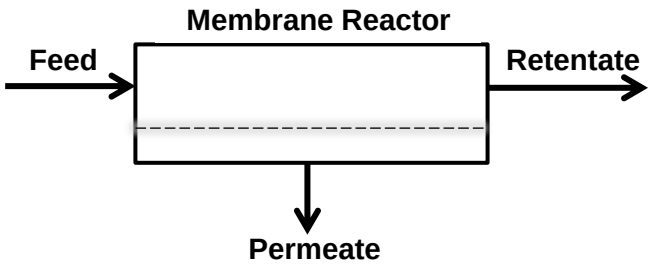

Figure 2.2- Schematic representation of a membrane process where the feed was separated into retentate and permeate.

The performance of a membrane is mostly determined by its selectivity and permeability. The permeation flux is a feature of the membrane and it is defined as the number of moles passing through the area of the membrane per time . On the other hand, the membrane selectivity towards gas mixtures is usually expressed in terms of a separation factor. For a mixture consisting of components A and B the selectivity (or separation) factor $\alpha_{A/B}$ is given by equation 2.1, where y_A and y_B are the concentrations of each component in the permeate and x_A and x_B are the concentrations of the components in the feed.

$$\propto_{A/B} = \frac{y_A/y_B}{x_A/x_B} \tag{2.1}$$

If the value of the selectivity is greater than the unit, it means the permeated flux of component A through the membrane is larger than the permeated flux of component B (the separation factor is denoted as $\alpha_{A/B}$); if component B permeation flux is higher than component A, then the factor is given by $\propto_{B/A}$. If $\propto_{B/A}$=$\propto_{A/B}$=1, no separation is achieved (Mulder, 1996).

2.1 METALLIC MEMBRANES

Membranes can be classified in different ways, namely based on their constitutive materials; according to that membranes can be classified into organic, inorganic and hybrids of organic/inorganic systems. Organic membranes can be either polymeric or biological in nature, while the inorganic ones can be made of metal or ceramic. But, as of this work, a metallic membrane was used during all the experiments of permeation test and reaction test (WGS) and for that reason will be the main focus of attention.

In the metallic membranes, hydrogen has to be dissociated into its components and, for this to be possible, both conduction of free electrons and a catalyst bed has to be provided. What happens is that hydrogen dissociates into protons and electrons still in the feed side (lumen side) and after the permeation, an association of those protons and electrons occurs so it is removed as molecular hydrogen (H_2).

In this work, the separation of the hydrogen was made through a palladium (Pd)-based membrane with silver, but there are also other alloys that could work for the same purpose (i.e., made of copper, for instance). This kind of membranes offer high surface reactivity for hydrogen separation, are resistant to embrittlement (structural change with hydride formation that occurs due to the solubility of the hydrogen in the membrane, this phenomenon resulting in the membrane failure) and high selectivity for hydrogen since their dense structure won't let any other molecules, particularly those larger than hydrogen, to go through. This feature is directly related with the high

purity of hydrogen that can be provided with metallic membranes. In such membranes, H_2 permeates through the solid material via the solution-diffusion mechanism (figure 2.3), which is described by the following steps:

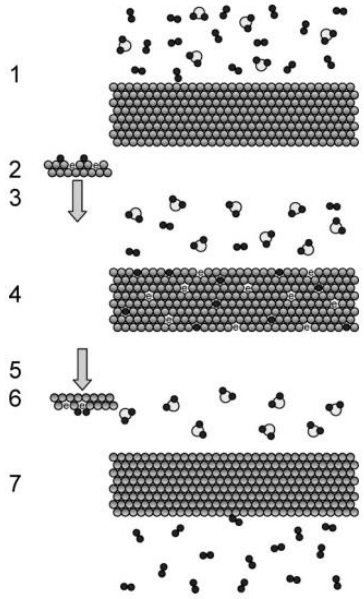

1. Movement of the raw gas to the feed stream surface of the membrane;
2. Dissociation of the chemisorbed H_2 into hydrogen ions (H^+) and electrons (e^-);
3. Adsorption of the H^+ ions into the membrane bulk;
4. Diffusion of the H^+ ions and electrons through the membrane;
5. Desorption of H^+ ions from the membrane bulk to the product stream surface of the membrane;
6. Association of the H^+ ions and electrons into discrete molecules of H_2;
7. Diffusion of the H_2 from the product surface of the membrane.

Figure 2.3 - Scheme of the solution-diffusion mechanism in a dense metallic membrane (Nenoff, 2007)

Diffusion through dense membranes is driven by a chemical potential concentration gradient across the metal lattice and is described as follows (McLeod, 2008):

$$J_{H_2} = -\frac{D \times C_{H_2}}{RT} \times \nabla \mu_{H_2} \tag{2.2}$$

Fick's law states that the diffusional flux of hydrogen species (J_{H_2}) is proportional to the diffusion coefficient (D) and the gradient of chemical potential of such species ($\nabla \mu_{H_2}$); T is the absolute temperature (K) and R the ideal gas constant (8.314 J mol^{-1} K^{-1}). In absence of significant gradients other than concentration (strain, temperature, etc.), the hydrogen permeated through a membrane per unit area and unit of time at a steady state and considering a constant diffusion coefficient is given by:

$$J_{H_2} = -D \frac{(C_p - C_r)}{t} \tag{2.3}$$

where *t* is the thickness of the membrane and the index *p* and *r* denote the permeate side and retentate side, respectively. Going one step further and assuming that the process of hydrogen diffusion through the membrane is much slower than the processes occurring in the membrane surface, a quasi-equilibrium state can be considered. On this matter, the hydrogen concentration into the metal is proportional to a solubility coefficient S (mol m^{-3} $Pa^{-0.5}$) and to the square root of

the hydrogen partial pressure. A generic form for the equilibrium concentration of absorbed gas can therefore be formulated as follows:

$$S_{H_2} = \frac{C_{H_2}}{P_{H_2}^{1/2}} \tag{2.4}$$

yielding for the H_2 flux:

$$J_{H_2} = -\ D_{H_2} S_{H_2} \frac{\Delta P_{H_2}^{1/2}}{t} = Pe \frac{P_{H_{2,r}}^{1/2} - P_{H_{2,p}}^{1/2}}{t} \tag{2.5}$$

where Pe is the permeability and $P_{H_{2,r}}$ and $P_{H_{2,p}}$ are the partial pressures of hydrogen on the feed stream and permeate side, respectively, S_{H_2} is the solubility coefficient of hydrogen and D_{H_2} is the diffusion coefficient of hydrogen. The hydrogen flux is dependent on the composition of the membrane, its chemical structure and thickness, and fabrication method (Santucci, 2011/2012).

The permeability coefficient (mol m^{-1} s^{-1} $Pa^{-0.5}$) is therefore given by:

$$Pe = S_{H_2} D_{H_2} \tag{2.6}$$

This permeability coefficient can be described as a function of temperature, according to an Arrhenius-type relation:

$$Pe = P_{e,0} e^{\left(\frac{-Ea}{RT}\right)} \tag{2.7}$$

being $P_{e,0}$ (mol m^{-1} s^{-1} $Pa^{-0.5}$) the pre-exponential permeability coefficient, and Ea (J mol^{-1}) the activation energy.

2.1.1 Palladium based membranes

Metal alloys are supposed to enhance several characteristics and overcome certain limitations of pure metals and, in the field of hydrogen separation, it is possible to think of two big groups: Pd-based and non Pd-based alloys.

Palladium is an ideal material for hydrogen separation mostly because it offers high solubility and diffusivity. However, Pd membranes may suffer from hydrogen embrittlement if operated at temperatures below 300 °C (figure 2.4). To overcome this issue, alloys (copper and silver, especially) are used.

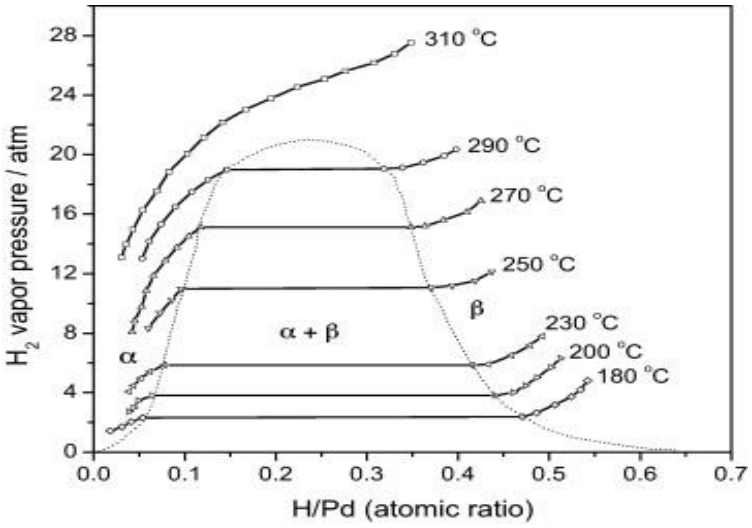

Figure 2.4 - P-C-T phase diagram of the palladium hydrogen system (Yun & Oyama, 2011).

Adding silver, particularly, with Pd, it results in a decrease of the critical temperature and pressure for the α→β transition. Also, there is an increase of the range of temperatures in which the membrane can be operated, without over worrying about the phenomenon of embrittlement.

At 350 °C and 2.2 MPa, the maximum value of hydrogen permeation is reached for the 23 wt. % Ag alloy and it is 1.7 times bigger than in pure Pd (Johannesen, 2014) making this alloy much more reliable than using pure palladium membranes.

Pd-alloys also offer a virtually infinite selectivity (figure 2.5) for hydrogen and increase the range of temperatures in which the membrane can be operated; moreover, they offer high reactivity for hydrogen dissociation and inherently improved permeability.

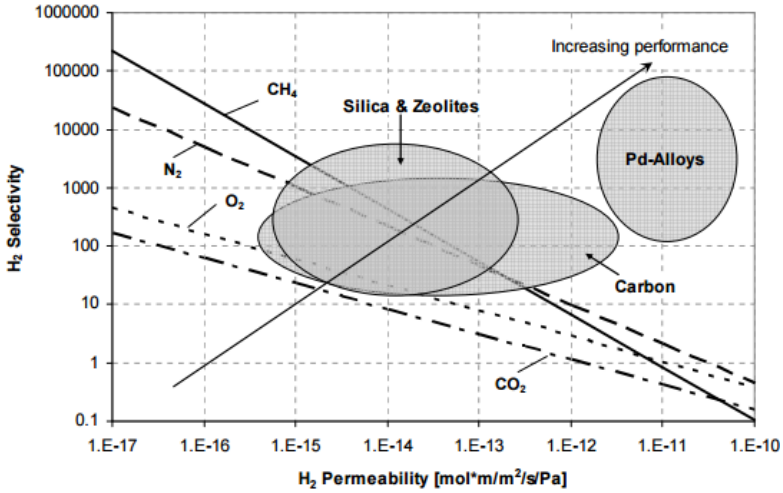

Figure 2.5 - Relative performance of the various H2 membrane materials (McLeod, 2008).

In his 1956 patent, Hunter revealed that alloying Pd with 27 mass % Ag not only prevented embrittlement on membranes, but enhanced the hydrogen permeability of the alloy by 70% too,

when compared to pure palladium at a temperature of 450 °C (USA Patente Nº US2773561 A, 1956). Also, alloys of Pd with Au and Cu have pure hydrogen permeability greater than pure Pd, they are unaffected by thermal cycling, and had some resistance to sulphur poisoning by hydrogen sulphide. Although, and as reported in figure 2.6, the absolute values of the permeability for these alloys are rather low when compared to Pd-23%Ag.

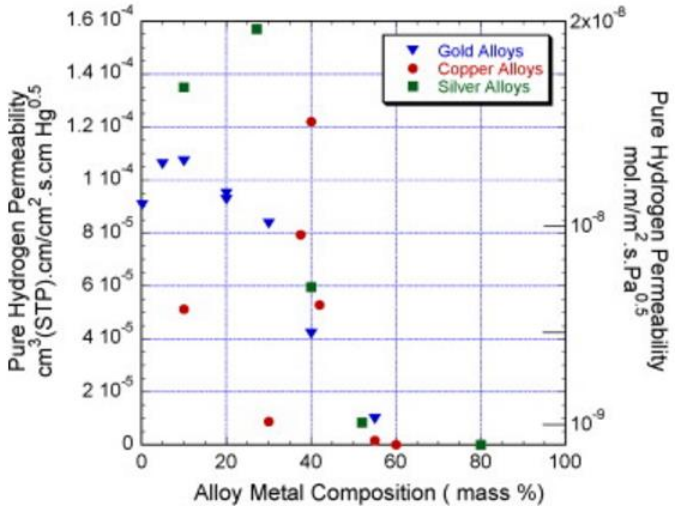

Figure 2.6 - The influence of alloy composition on the pure hydrogen permeability for Pd-alloy membranes containing Au, Cu and Ag at 350°C (Hatlevik, 2010).

3 WATER GAS SHIFT REACTION

The water gas shift is an important industrial reaction that is accompanied - most of the times - with steam reforming, in which hydrocarbons react at high temperatures to produce hydrogen. This reaction is moderately exothermic and reversible, so high equilibrium conversions can be achieved at lower temperatures. Moreover, it is characterised by no variation in the number of moles ($CO + H_2O \leftrightarrow CO_2 + H_2$ and $\Delta H^{\circ}_{298} = -41.1\ kJ.mol^{-1}$).

This reaction is also a very attractive option to clean greenhouse gases such as CO, in exchange of high-purity H_2 production that could be used in fuel cells. Overall, WGS reactors with integrated Pd membranes are also an interesting option for pre-combustion CO_2 capture in large-scale from fossil fuels power generation (Miao, et al., 2017).

As above mentioned, the CO equilibrium conversion is favoured by low temperatures and is independent of the reaction pressure when operating in a conventional reactor. On the contrary, in a Pd-based membrane reactor a high pressure on the reaction side facilitates the hydrogen permeation and, therefore, the operating temperature can be reduced because the equilibrium is shifted towards the products formation. Furthermore, the required amount of catalyst can be significantly reduced as well.

To promote WGS reaction, it is needed to provide a catalyst bed and, particularly in ENEA, a group of catalysts was already tested for this purpose, which are, among others, Platinum based catalysts (non-commercial, from Argentina), Platinum based with alumina support and, more recently and presented in this work, a copper based catalyst. These three catalysts will be described later on and are also to be compared later in this work.

3.1 CATALYST

Catalysts are extremely important on chemical reactions, being the material that speeds it up. With the catalyst molecules that might take years to interact, will do so in a matter of seconds. Factories rely on catalysts to make everything from drugs to plastic, helping also to process petroleum and coal into liquid fuels.

During any chemical reaction, molecules break the chemical bonds between their atoms. These breaks may not be easy and catalysts make such breaking and rebuilding happen more efficiently and quickly. They do this by lowering the activation energy of a chemical reaction.

Even if it is so useful in chemical reactions, catalysts are not consumed upon use.

The catalyst used in this experimental work, as mentioned before, was a commercial copper based medium temperature WGS catalyst**, HiFuel ® W230**; prior to use, it is required to know the specifications of the catalyst and its handling procedure, based on the supplier's indication:

Feed quality: This catalyst is susceptible to sulphur, chloride and silica poisoning and should be protected from these components by upstream purification.

Activation: Supplied in non-reduced form, a controlled activation was required under reducing conditions above the dew point. The reducing agent concentration should be less than 2% mole dry, and the temperature should be maintained at < 230 °C.

Handling: Once reduced, the catalyst is pyrophoric. Prior to discharge the catalyst should be exposed to steam and oxidised. It is to be avoided any contact with skin and clothes and it is also to be avoided breathing dust.

Copper based catalysts are a good low cost option for low to moderate WGS reactions temperature, but there are also a few step-backs when handling and using them. This kind of catalysts are very sensitive to oxygen exposure and they may suffer from some thermal deactivation. They can also suffer from sulphur and chlorine poisoning and require a careful reduction process.

4 EXPERIMENTAL SETUP

The tests presented below in this thesis (permeation test and reaction test with WGS reaction) were performed using a membrane reactor. Figure 4.1 is a schematic representation of the plant of the membrane reactor used for both procedures.

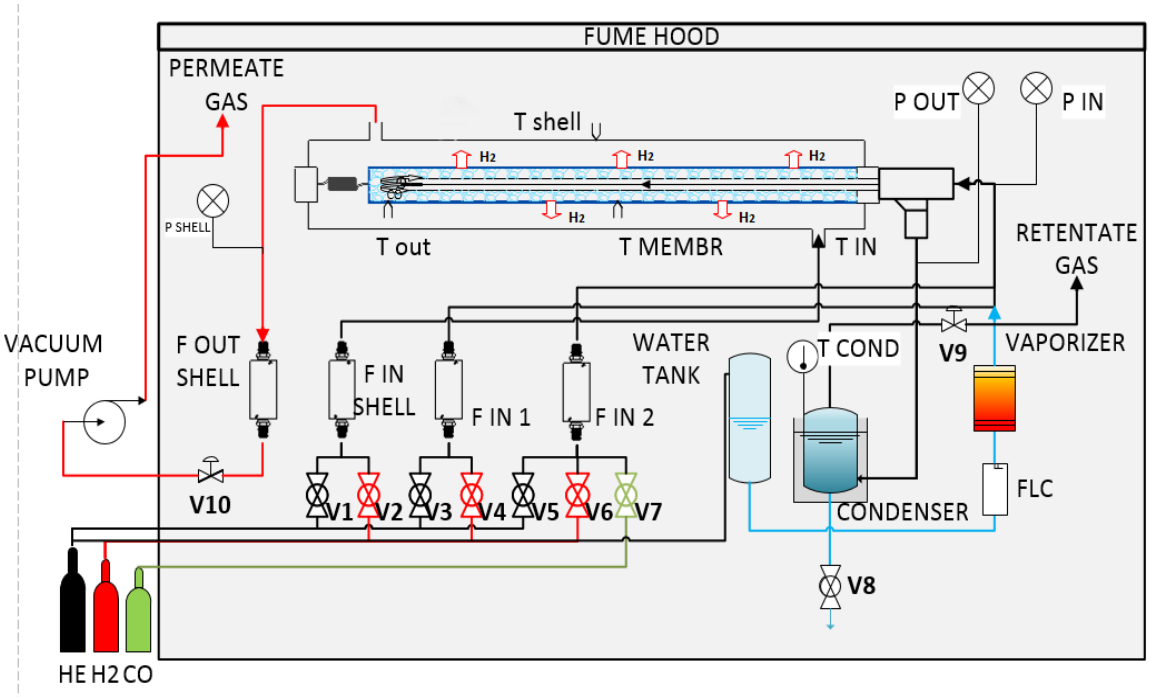

Figure 4.1 - Experimental Plant of the Reactor (Autor: Incelli, M. 2016).

This membrane reactor was made of a Pd-Ag (25% wt. Ag) single tube with a wall thickness of 142.9 µm, length of 500 mm and diameter of 10 mm. The same tube is fixed only by one side, while the other side is connected to a spring that assures the elongation of the membrane, preventing the stress in its surface. The metallic spring has an outside diameter of 15.2 mm and the force applied to the membrane was about 40 N which corresponds of an elongation of roughly 28 mm.

During both tests (permeation and reaction), the stream was fed to the lumen side of the membrane, while the permeated hydrogen was collected in the shell side of the membrane with the assistance of a vacuum pump.

The volumetric flow rate of all the gases fed to the membrane was monitored and adjusted by mass flow controllers with a range between 0 and 500 sccm. Two of these mass flow controllers are located in the gas feeding, so it was easy to control the feeding flow rate of helium, hydrogen

and CO altogether in both permeation and reaction tests. There was another mass flow meter which measured the flow of the permeated hydrogen. There is also a liquid flow controller that assisted on the amount of water that was fed to the reactor on the reaction tests.

This water was kept in a pressurized tank with helium and fed to the membrane reactor by pressure difference, passing through a resistance that heated the amount of water up to 200 °C. Also, as the reaction test was being performed, there was a cold trap around a condenser, made out of alcohol, water and liquid nitrogen, which allowed the gases from the retentate side to be dried, collected and, subsequently, analysed with a gas chromatograph.

The membrane itself was heated by letting the current pass directly through it. The current was regulated manually, starting that procedure by setting the maximum voltage at a value not over 5 V.

Moreover, the pressure measurements were taken by different barometers located in different parts of the system – two of them are located at the entrance and the exit of the membrane (lumen – feed and retentate side), with a range of measurement up to 10 bar. Another one intercepted the outline of the shell side (permeate side) and it had an upper limit of 1 bar and a lower limit of 10^{-4} bar.

All the experimental data was collected with the software LabView that displayed data in real time and recorded in a digital format. This software allowed not only the monitoring of the whole system but also shows the temperature and pressures graphically and numerically. It also allowed the regulation of the values of the feed stream directly from the interface of the program.

The starting up procedure of the experiments (including the software and membrane preparation) as well as the cooling down procedure and leak test are described in the Appendix C.

5 PERMEATION TESTS

The permeation tests, as mentioned before, aimed the experimental determination of the hydrogen permeability of the Pd-Ag membrane under different operating conditions (pressures and temperatures). Particularly, in this work it was first assessed the hydrogen permeability of the Pd-Ag membrane and then the hydrogen permeation flux through the membrane when it was fed with a gas stream containing different H_2/He molar ratios; the goal was to establish a general trend of the hydrogen permeation flux at different hydrogen partial pressures differences. For that, a mixture of hydrogen and helium was fed at different temperatures (250 °C, 300 ºC, 350 ºC and 400 ºC), molar ratios and pressures.

The hydrogen permeability through the membrane is calculated by Sieverts' law equation, showing the permeability as a function of partial pressure and hydrogen flux permeated:

$$Pe = \frac{J\,t}{P_{H_2}^{0.5} - P_{H_{2,shell}}^{0..5}} \tag{5.1}$$

During the permeation tests the amount of helium and hydrogen was adjusted to different ratios of H_2/He, therefore providing different partial pressures inside the membrane.

5.1 CONDITIONS

In the first part of this work – the permeation tests – the H_2/He molar feed ratio was varied. So, in order to operate at the desired H_2/He ratio, the membrane was fed with the He and H_2 flow rates reported in Table 5.1.

Table 5.1 - Operational conditions for the permeation tests (flow rates and ratios)

Tests	H_2 Flow Rate [sccm]	He Flow Rate [sccm]	Ratio H_2/He [sccm]
Run #1	400	50	8
Run #2	200	200	1
Run #3	50	400	0.125

For each one of the He/H_2 feed molar ratios reported in Table 5.1, all the following conditions of lumen pressure and membrane temperature have been tested (Table 5.2).

Table 5.2 – Experimental conditions inside the reactor (Membrane temperature and Lumen pressure)

Parameters	**Values**
Lumen pressure [bar]	1, 2, 3, 4, 5
Shell pressure [bar]	10^{-4} to 10^{-1}
Membrane temperature [°C]	250, 300, 350, 400

The shell pressure varies essentially because of two factors:

- The pumping speed is constant, therefore in case of different permeation flux the value of the final pressure could be different;
- The needle valve before the pump is partially closed/opened.

A total of 69 tests have been performed. For each test, pressures, temperatures and flow rates values have been averaged over the whole duration of the test. Each test lasted at least 30 minutes in stable conditions (i.e., upon steady-state has been reached). The leak tightness of the membrane has been checked daily (i.e. after each 5 tests) by pressurizing the lumen with helium. Within the entire experimental campaign, none leak has been detected in the membrane module.

5.2 Results and Discussion

The results of the permeation tests were analysed in terms of permeability and H_2 permeation flux. Firstly, the membrane permeability has been evaluated through equation (5.1). Figure 5.1 shows the dependence of the logarithm of the permeability from the inverse of the absolute temperature. The dependency is characterized by a linear trend, as expected (Arrhenius behaviour), particularly at lower pressures; it becomes however nearly constant at higher temperatures

All the graphs with the permeation flux vs. driving force are represented in appendix A. Moreover, these figures show how the data fit the Sieverts' law.

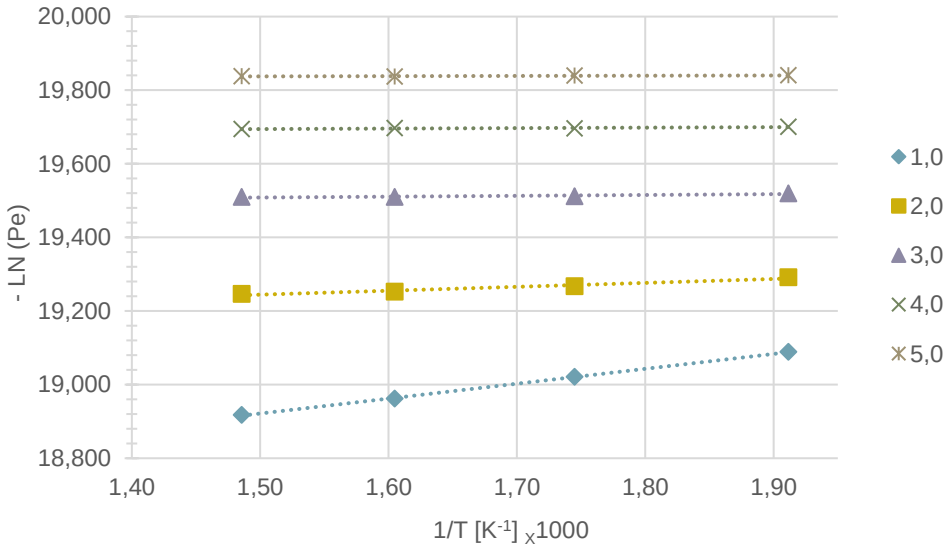

Figure 5.1 - Measured permeability at different pressure conditions for He/H_2=1 (feed ratio).

The table below presents the results obtained in this work and the published ones of the activation energy (E_a) and pre-exponential factor (Pe_0) calculated with the Arrhenius Law (equation 2.7) with operating conditions such as pressure of the tests, as well as tested membrane thickness.

Table 5.3 - Published results of Pre-exponential factor and activation energy

Lumen Press. [kPa]	Thickness [µm]	Ea [kJ/mol]	Pe0 [mol/(m s $Pa^{0.5}$)]	Feed flow	Ref.
100	142.9	3.365	1.11 x 10^{-08}	50% H2 and 50% He	This work
100	200	8.086	8.78 x 10^{-8}	Pure hydrogen	(Tosti, Borgognoni, & Santucci, 2010)
200	150	2.566	1.09 x 10^{-08}	Pure hydrogen	(Santucci, Borgognoni, Vadrucci, & Tosti, 2013)
200	84	3.610	3.33 x 10^{-08}	Pure hydrogen	(Santucci, Borgognoni, Vadrucci, & Tosti, 2013)

The results obtained in the present work are in line with the ones published previously.

As already introduced, in these permeation tests the membrane lumen was fed with different H_2/He feed molar ratios. So, the results are presented below in terms of permeation efficiency (η). The permeation efficiency is defined as follows:

$$\eta\ (\%) = \frac{F_{H_2 Permeated}}{F_{H_2 in}} \times 100 \tag{5.2}$$

being $F_{H_2 Permeated}$ the amount of hydrogen that permeates through the membrane and $F_{H_2 in}$ the amount of hydrogen that is fed to the membrane tube. The main contribution for the hydrogen permeation, and therefore accounting for a higher or lower permeation efficiency, is the hydrogen partial pressure in both sides of the membrane (commonly called the driving force). In equation 5.3 is characterized this driving force as the difference of the square roots of the hydrogen partial pressures, as shown in equation 5.1, referred as Sieverts' Law.

$$\Delta P = P_{H_2\, lumen}{}^{0,5} - P_{H_2\, Shell}{}^{0,5} \tag{5.3}$$

The following figures (5.2, 5.3 and 5.4) represent graphically the results for the permeation efficiency for the molar ratios H_2/He of 8, 1 and 0.125, respectively.

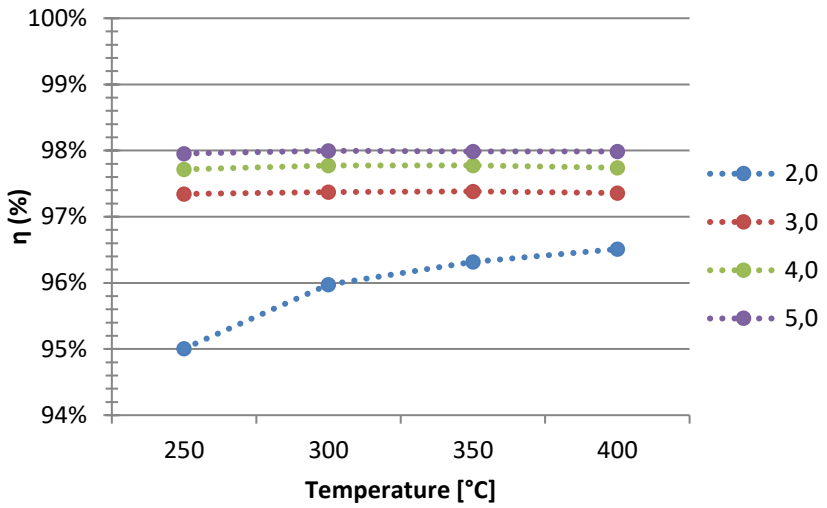

Figure 5.2 – Permeation efficiency for each lumen pressure and temperature tested at H_2/He=8.

.

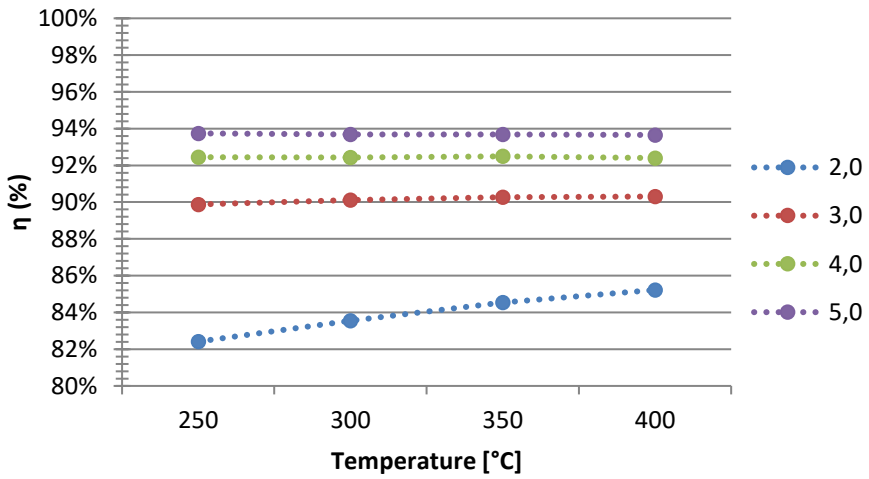

Figure 5.3 - Permeation efficiency for each lumen pressure and temperature tested at H_2/He=1.

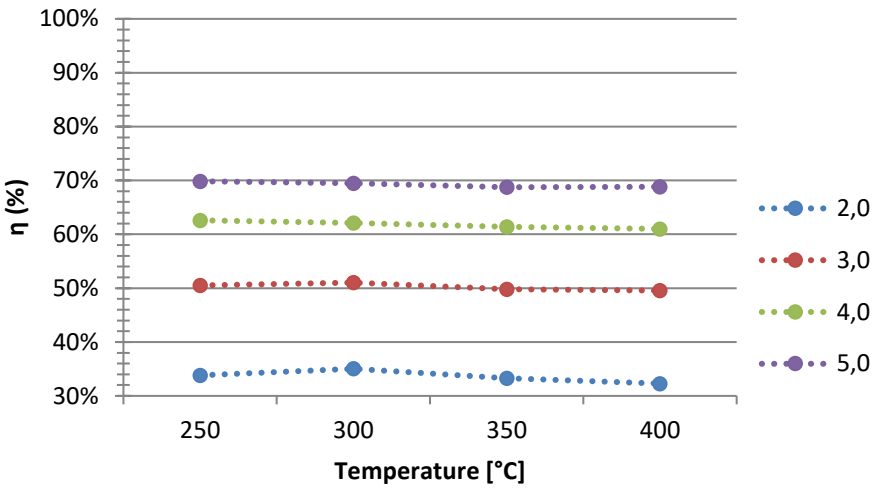

Figure 5.4 - Permeation efficiency for each lumen pressure and temperature tested at H_2/He=0.125.

In the graphics of the figures 5.2, 5.3 and 5.4, we can observe that the temperature almost does not influence the permeation efficiency, at least in a relevant way (except for the lumen pressure of 2 bar and H_2/He molar ratios of 8 and 1). Also, at lower H_2/He molar ratios the temperature effect is almost negligible. This evidences that the total pressure in the lumen side of the membrane is a more relevant operating condition, as well as the composition of the feed stream (one can see that for strongly diluted streams, namely for an H_2/He molar ratio of 0.125, the permeation efficiency is considerably detrimentally affected because this way the driving force for hydrogen permeation is smaller).

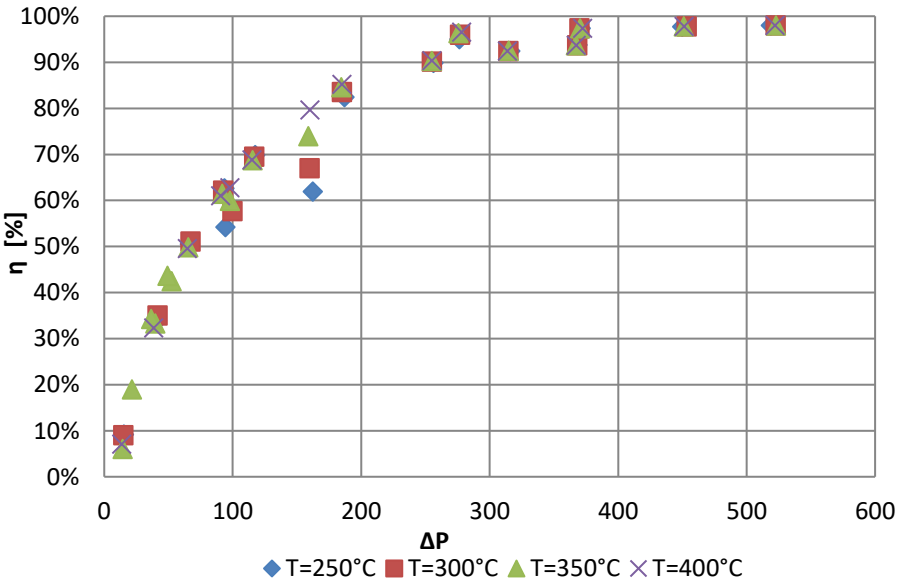

Figure 5.5 - Hydrogen permeation efficiency per the driving force (ΔP) at each tested temperature

In figure 5.5 are compiled all the results for efficiency vs. the driving force. This figure is a very useful resource for further use when it comes to know how much pressure we need to apply on the membrane to obtain a certain amount of hydrogen permeation/recovery.

6 WATER GAS SHIFT: REACTION TESTS

In this section, it is described not only the conditions in which the membrane reactor was ran but also all the results of it, including efficiency of the system and the amount of the impurities that were collected on the retentate side.

CO and H_2O feeds are usually tested in membrane reactors (MRs) for the water gas shift reaction, particularly in the Pd-Ag "finger-like" self-supported membranes, like the one this work was performed in, conceived specially for the ultra-pure hydrogen production. In the present work, the CO and H_2O feed stream was converted at the temperatures of 250, 300 and 350 °C with pressures from 2 bar up to 5 bar in a molar proportion of $H_2O/CO = 1$. With the same feed ratio, there was another test ran at 300 °C with pressure going from 2 up to 5 bar and then from 5 bar down to 2 bar to verify the results obtained, since it was verified an apparently-unjustified peak at a lumen pressure of 3 bar, that stands out of the trend of the results obtained for this temperature in terms of efficiency and gases analysed on the GC. Therefore, there was needed to repeat the experiment with a cycling that would test the catalyst stability and the reproducibility of the results.

6.1 CATALYST

As said before, the catalyst used in this experimental work was a **copper based medium temperature WGS catalyst**, HiFuel ® W230. The catalyst has a cylindrical shape with the size of 5.5 x 3.6 mm and it is recommended for temperatures from 200 °C (minimum) up to 350 °C (maximum). When it comes to the pressure, it has a minimal impact.

The first step towards the water gas shit reaction (WGSR) tests was to define the conditions it should be operated in taking into consideration the recommendations of the manufacturer. Afterwards, the catalyst had to be inserted inside the reactor. The Cu based catalyst, HiFuel ® W230, had to be grounded into smaller pieces, since the diameter of the original pellets were too large for the space available (0.4 cm on each side of the tube) inside the reactor. Each piece of Cu based catalyst had a size of ≈2 mm. A total of 16 g of grounded Cu based catalyst was inserted inside the tube along with glass spheres to avoid temperature gradients.

Later, the catalyst had to be activated. The manufacturer's specifications determined that it had to be activated with 2% mol. dry of hydrogen using helium as carrying gas. Table 6.1 shows the ratio of H_2/He used in this activation as well as the activation conditions. This activation procedure lasted around 3 hours.

Table 6.1 - Catalyst activation conditions

	Hydrogen Flow Rate [sccm]	Helium Flow Rate [sccm]
2% mol. dry	10	500
Temperature [°C]	230	
Pressure [bar]	1	
Activation time [hours]	≈ 3	

6.2 WATER GAS SHIFT CONDITIONS

The water gas shift reaction was performed varying the temperature of the membrane and the pressure on the lumen side of the membrane. The feed conditions were chosen based on previous experiments executed in ENEA, with different catalysts, so that a comparison among those could be possible.

The amount of H_2O and CO fed to the reactor were calculated using the stoichiometric ratio on the following chemical reaction:

$$CO + H_2O \rightleftharpoons CO_2 + H_2$$

In table 6.2 are shown all the conditions used during every phase of the reaction test.

Table 6.2 – Reaction test conditions

	H_2O/CO = 1	
	mH2O [g/h]	mCO [sccm]
	4.50	93
T [°C]	250; 300; 350	
P [bar]	2; 3; 4; 5	

The first phase of these reaction tests was an investigation on the influence of the temperature on the reaction (knowing, before-hand, that the pressure does not affect the reaction itself, from the thermodynamic point of view, neither the catalyst is influenced by it). The range of temperatures were chosen according to the minimum temperature of the catalyst's best performance range and the highest temperature, going up to 300 °C and finally 350 °C that was the maximum value established by the manufacturer of the catalyst.

6.3 Water Gas Shift: Results and Discussion

All the results presented in this chapter are expressed in terms of efficiency (η) of the system (constituted by the membrane, the catalyst and the reactor itself), which is defined as the number of moles permeated through the membrane per unit time divided by the maximum number of moles that would be theoretically produced in the same time basis if all the CO was converted (equation 6.1).

$$\eta = \frac{mol\ of\ H_2\ permeated}{mol\ of\ H_2\ theoretically\ produced} \times 100 \qquad (6.1)$$

Also, the gases in the retentate side were collected and analysed with the Gas Chromatographer (GC) and using the calibration curves reported in the appendix B.

6.3.1 Influence of the temperature

In the first set of tests, the efficiency of the system has been measured at different reactor temperatures (at 250°C, 300°C and 350°C). In order to analyse the results, it is important to remember that the temperature has a beneficial effect on the permeation (i.e. the higher is temperature, the higher is the hydrogen permeation), while the water gas shift, being a moderately exothermic reaction, is promoted at low temperatures - from the thermodynamic point of view -, while reaction kinetics is accelerated at higher temperatures.

In figure 6.1 there is a clear vision of the influence of the temperature and the lumen pressure on the efficiency of the system.

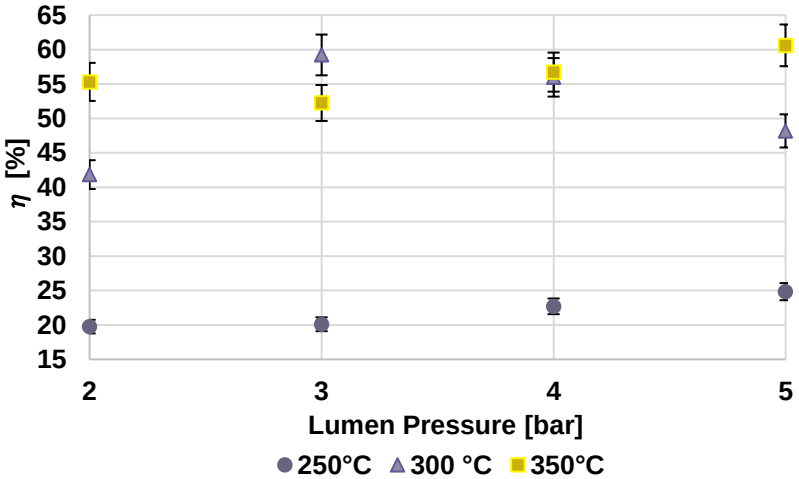

Figure 6.1 – Efficiency of the system at the temperatures of 250, 300 and 350 °C, at different lumen pressures

In general, it is possible to observe that by increasing the temperature the efficiency of the system increases, while the lumen pressure does not significantly affect the performance of the system. Particularly from 250 °C to 300 °C the efficiency goes from 20-25% up to 40-60%. The maximum efficiency of the system was roughly 55 % at a temperature of 350°C, which was pretty much constant during all range of pressure.

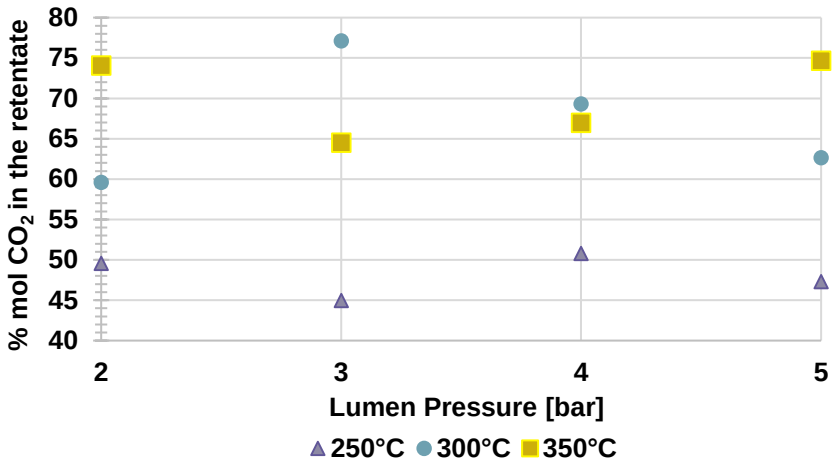

Figure 6.2 – Dioxide Carbon percentage in the retentate side using WSGR at a temperature of 250°C, 300°C and 350°C

About the gases collected on the retentate side and analysed in the GC, and starting with the carbon dioxide (Figure 6.2), it is possible to say that the amount of CO_2 pretty much follows the trend of results of the efficiency. Being CO_2 a product of CO conversion, as the efficiency increases, the amount of CO_2 in the retentate side/products will also increase and vice-versa. This feature allows us to know that the reaction is occurring as expected, although some deviations are seen in Figure 6.2. But for further discussion on this topic, it is necessary to know what happens also in terms of H_2 and CH_4 (see Figures 6.3 and 6.4).

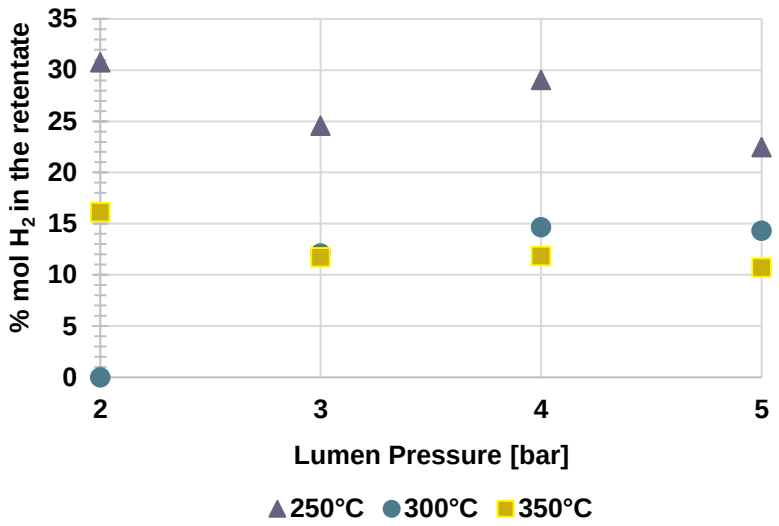

Figure 6.3 – Hydrogen percentage in the retentate side using WSGR at a temperature of 250°C, 300°C and 350°C

The optimal view of the MR performance would be the efficiency going up and the hydrogen in the retentate side going down, meaning that all the hydrogen produced in the WGS is permeating the membrane. The GC analysis reveals that in most cases, the retentate stream contains hydrogen – Figure 6.3. This means that not all the hydrogen produced by the WGS reaction is able to permeate through the membrane. Particularly, at 250 °C, the retentate contains up to 30 %mol. of hydrogen. This can be easily explained by considering that the permeability is a temperature activated phenomena and high hydrogen permeability values can be attained only when the membrane temperature is above 300 °C.

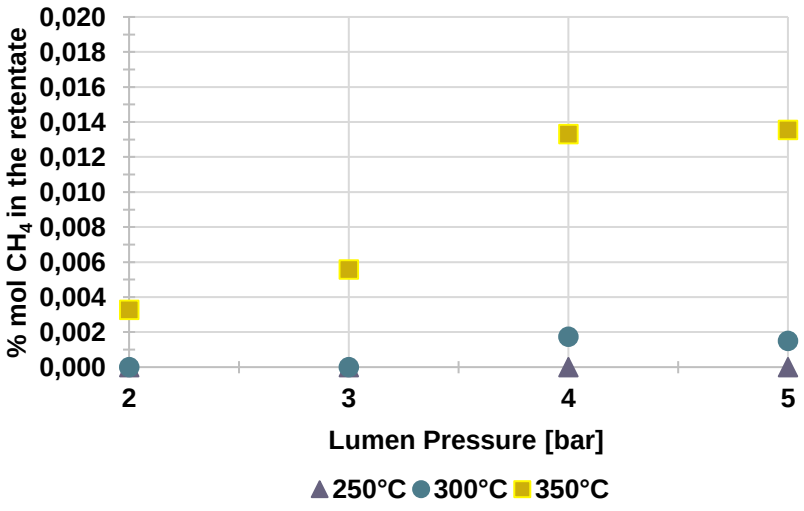

Figure 6.4 – Methane percentage in the retentate side using WSGR at a temperature of 250°C, 300°C and 350°C

Another important information is related to the amount of CH_4 in the retentate side. In fact, methane is the product of some secondary reactions that we should avoid (considering that our scope is to maximize hydrogen formation and recovery). As shown in Figure 6.4, in most of the operating conditions the methane formation was below the GC detectable limit, which represents good results for the Cu-based HiFuel ® W230 catalyst. Although, it is possible to observe a slight increase of the methane amount as the temperature goes up, confirming that the optimal working temperature of the catalyst, from the selectivity point of view, is about 250 °C as indicated in its specifications.

6.3.2 Catalyst cycling

After analysing the first series of results of the reaction tests it has been observed that the experiments at 300 °C did not perfectly match the trend of the results in a general picture. Taking that information into account, the second step of the reaction experiments was to repeat the tests at 300 °C changing the lumen pressure from 2 bar up to 5 bar and then, in the reversed order (from 5 bar down to 2 bar) to test the catalyst stability and the reproducibility of the results. However, before starting this second series of reaction tests both permeation test and catalyst regeneration have been repeated. The first aimed to check the presence/absence of any membrane poisoning effects (resulting from any species that could have remained on the membrane and that could affect its permeability towards hydrogen) and, the second, to be sure that the catalyst was not de-activated in the first part of the reaction test. Table 6.3 illustrates the permeability values measured before the first and the second reaction tests. The conditions of the new permeability test were chosen among the options already studied previously in this work, simply to compare if they matched. According to the results reported in the table below, there is almost no permeation decrease, and so, apparently, the membrane was not poisoned.

Table 6.3 - Results of the permeation tests before and after the reaction test.

Permeability [mol m^{-1} s^{-1} $Pa^{-0.5}$]	
T=350 °C / P=3 bar	
Permeation test (before)	3.37 x 10^{-09}
Permeation test (after)	3.28 x 10^{-09}

The catalyst regeneration conditions were the same as expressed in table 6.2.

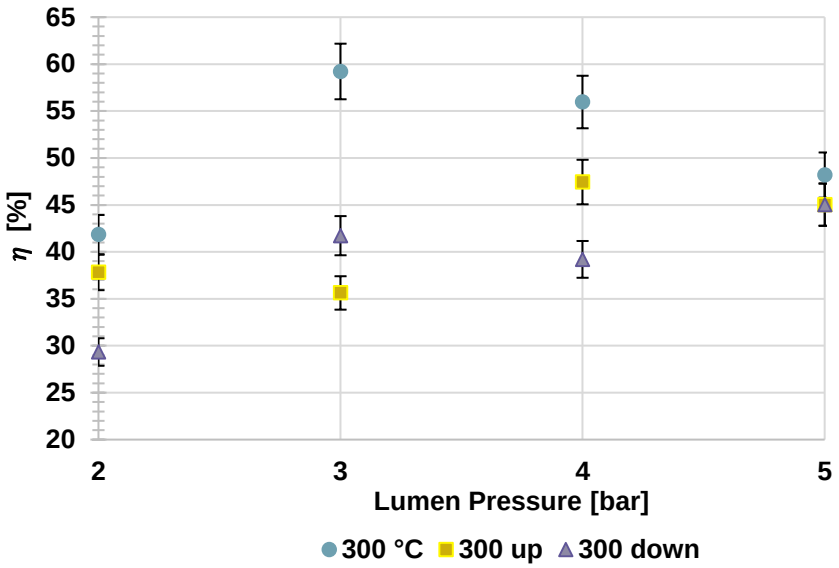

Figure 6.5 -Efficiency at 300°C before the permeation test (Normal) and after the permeation test going up from 2 to 5 bar (Up) and down from 5 to 2 bar (Down).

Figure 6.5 illustrates the efficiencies measured in the three tests performed at 300 °C: in blue are the results of the first reaction tests at 300 °C, while in yellow and in purple the results of the second tests at 300 °C obtained by increasing the lumen temperature (300 up in yellow) and by decreasing the lumen pressure (300 down in purple). Although all the results follow the same trend, the efficiency measured in the first series (300°C) is higher than in the second series (300 up and 300 down).

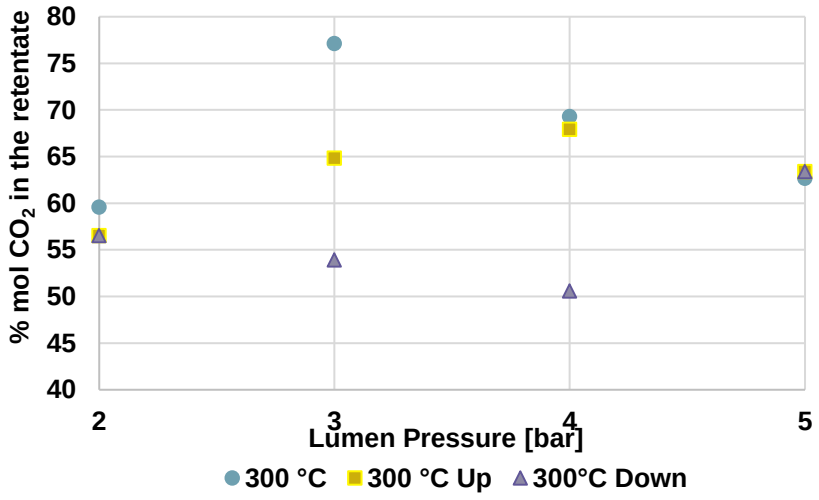

Figure 6.6 – Carbon dioxide percentage in the retentate side using WSGR at a temperature of 300°C (before the permeation test) and varying the pressure from 2 to 5 bar (300°C Up) and reversed (300°C Down).

The amount of CO_2 contained in the retentate side follows approximately the trend of the efficiency shown in figure 6.5 for each test: as the efficiency goes up, also the amount of CO_2 goes up.

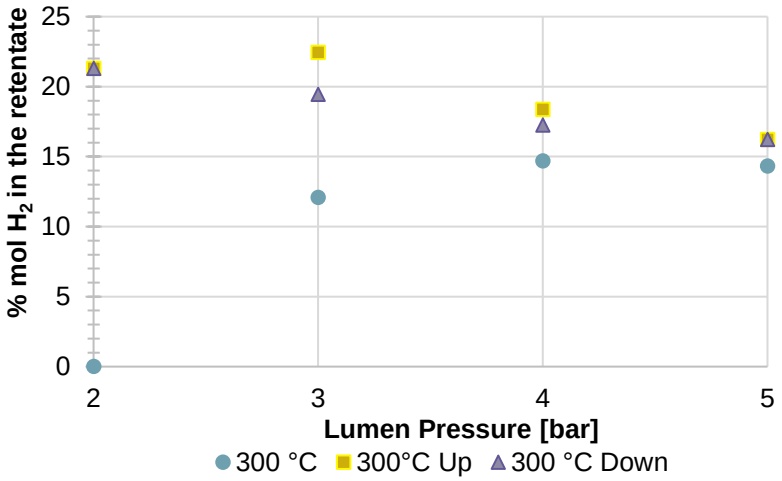

Figure 6.7 – Hydrogen percentage in the retentate side using WSGR at a temperature of 300°C (before the permeation test) and varying the pressure from 2 to 5 bar (300°C Up) and reversed (300°C Down).

The reason of the different results obtained in the tests at 300 °C is finally given by analysing the GC results related to the H_2 amount in the retentate. As shown in Figure 6.7, the amount of hydrogen in the retentate in much lower in the first reaction tests series than in the second. Being the permeability of the membrane constant, we have had checked the pressure in the permeate side of the membrane, which is regulated by a vacuum pump connected to the system via a needle valve. The values of the pressure in the permeated side in the different tests are reported in Table 6.4. It is possible to observe that in the first tests at 300 °C the shell pressure was considerably lower than in the other tests. Of course, this fact has a direct consequence on the hydrogen permeation flux since the higher is the pressure difference between the shell and lumen side, the more hydrogen permeates trough the Pd membranes.

Table 6.4 - Shell pressure in all the tests at 2 bar lumen pressure

Pshell [bar]			
Lumen Pressure [bar]	**Temperature [°C]**		
	300	300 up	300 down
2	6.26×10^{-02}	1.3×10^{-01}	1.34×10^{-01}

In other words, the pressure in the shell side on the two last tests is pretty much the same, but in the first series of tests the pressure in the shell side is lower. This fact translates into a better condition for hydrogen to permeate through the Pd-Ag membrane (so less H_2 is seen in the retentate side in the first series of experiments – Fig. 6.7) and, therefore, an increase of efficiency as shown in figure 6.5. Finally, if more hydrogen permeates through the membrane in the first series of experiments, the WGS is further shifted into the products side, and inherently more CO_2 is formed (cf. Fig. 6.6).

When it comes to CH_4, figure 6.8 illustrates the gas chromatograph (GC) results on all the three tests.

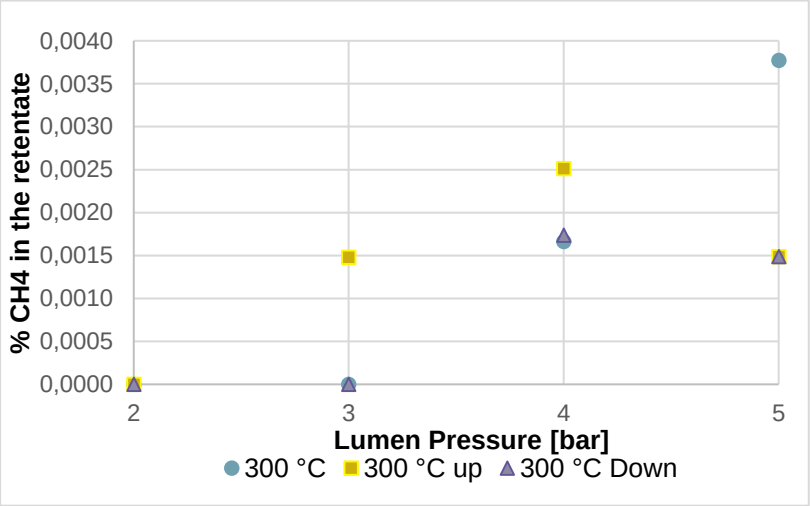

Figure 6.8 – Methane percentage in the retentate side using WSGR at a temperature of 300°C (before the permeation test) and varying the temperature from 2 to 5 bar (300°C Up) and reversed (300°C Down).

The methane amount in the retentate is very low in each test series. At this kind of low range, it is not easy to discern the values.

6.4 WATER GAS SHIFT: DIFFERENT CATALYSTS

As a last analysis of the results, a comparison among catalysts was carried out; this was possible because of previous tests that were made at ENEA. The catalysts 1 and 2 were tested previously at ENEA by Marco Incelli while the third catalyst was the one tested in this work.

Table 6.5 – Catalyst properties

CAT 1	• Non-commercial catalyst (Synthesized by Instituto de Investigaciones en Catálises y Petroquimica) • Pt (0.62 wt.%), SiO_2 (56.32 wt %). • Pellets (from 1x1x1 mm to 4x2x1 mm)
CAT 2	• Commercial catalyst (Produced by BASF) • Pt-based dry unreduced catalyst (Pt 1 wt.% on alumina support, SP-01 T) • Pellet of 1.5x1.5 mm cylindrical shape
CAT 3	• Commercial Catalyst (produced by HiFuel ®) • Cu based medium temperature WGS catalyst (HiFuel ® W230) • Pellet of 5.5 mm x 3.65 mm, cylindrical shape

The conditions in which the experiments with the catalysts described in table 6.5 were performed were exactly the same in terms of amount of feed gas/water fed to the membrane, lumen pressure, membrane dimensions and range of temperatures. The only difference was on the pressure on the permeated/shell side in which CAT 1 and 2 were performed on a magnitude of 10^{-2} bar and the tests with CAT 3 were performed at a pressure of 10^{-1} bar. This fact might relevant when analysing the results presented below.

6.4.1 Results comparison among different catalysts

The results presented next are expressed in terms of efficiency and amount of methane and carbon dioxide in the retentate side.

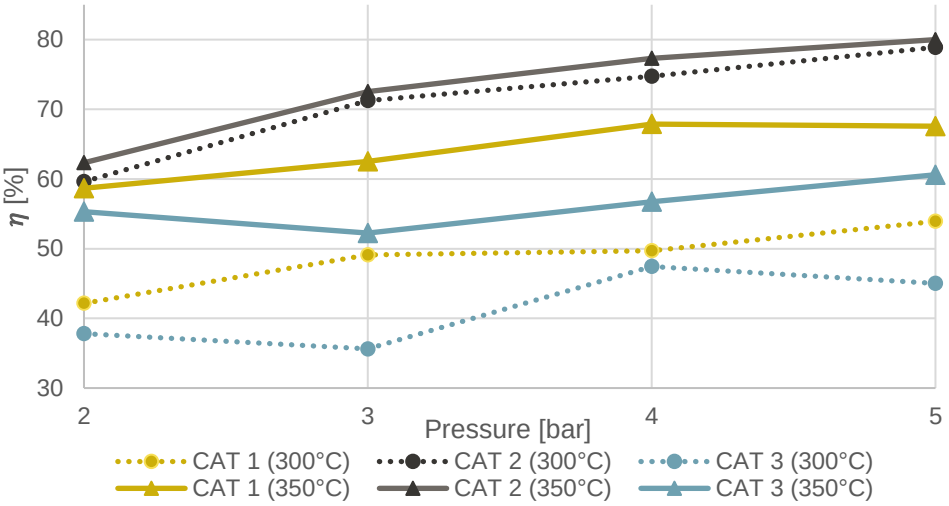

Figure 6.9 - Efficiency of the system using three different catalysts [Cat 1 – Non-commercial Platinum and silica; Cat 2 – Commercial catalyst (BASF) Platinum based with alumina support; Cat 3 – Cu based commercial catalyst (tested in this work).]

The efficiency obtained with the Cu-based catalyst (tested in this work – CAT 3) is rather low compared with the efficiency obtained with previous catalysts, as shown in figure 6.9. The best catalyst – efficiency wise – is the catalyst number two (Pt-based catalyst with alumina support) in both of the temperatures considered for comparison.

But, another important aspect to be considered is the presence of methane as by-product. So, the following graphics show the comparison of produced methane and CO_2, for each catalyst tested.

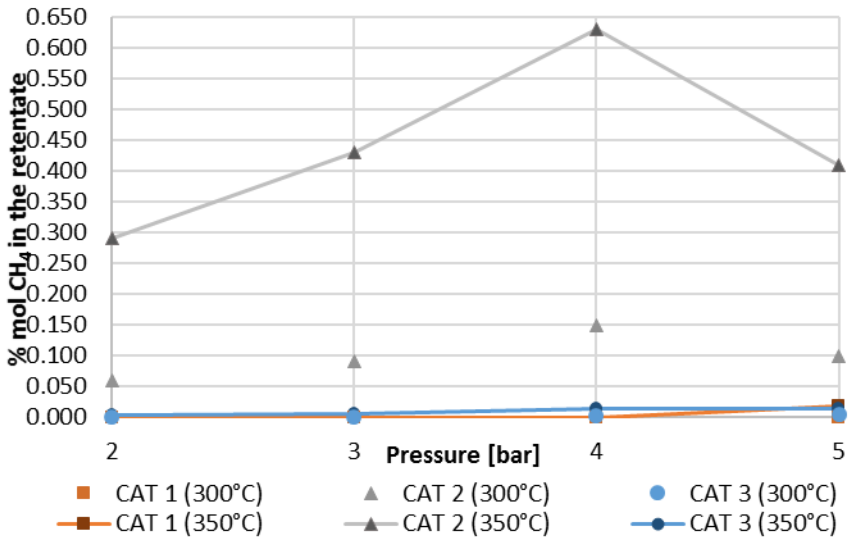

Figure 6.10 – CH_4 in the retentate side from WSGR using three different catalysts [Cat 1 – Non-commercial Platinum and silica; Cat 2 – Commercial catalyst (BASF) Platinum based with alumina support and Cat 3 – Cu based commercial catalyst (tested in this work).]

Despite the high efficiency of the second catalyst, the high amount of methane formed makes it unreliable in comparison to the other two. Being the goal of these experiments to find the best catalyst in terms of lower methane production, the better choice would be either the first or third catalyst.

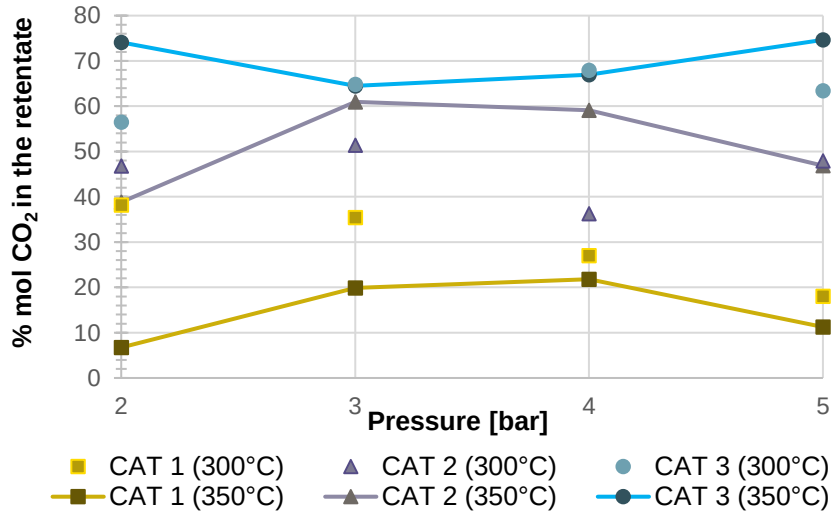

Figure 6.11 – CO_2 in the retentate side from WSGR using three different catalysts [Cat 1 – Non-commercial Platinum and silica; Cat 2 – Commercial catalyst (BASF) Platinum based with alumina support; Cat 3 – Cu based commercial catalyst (tested in this work).]

As a direct consequence of CO conversion via WGSR, the increase of CO_2 shows the catalyst performance. Considering such, the catalyst number 3 (copper based catalyst studied in this work), shows a better result in this aspect, outperforming the other two. This information is valid for both

temperatures (300°C and 350°C). The Cu-based catalyst, however, showed a lower efficiency when compared to the other two, which may be explained by the fact that both CAT 1 and 2 were tested at a shell pressure (permeate side) of 10^{-2} bar, whilst the CAT 3 was performed in a 10^{-1} bar (in the latter the lower driving force is responsible for the lower hydrogen recovery observed).

7 CONCLUSIONS

The tested WGS MR system has a better efficiency as the temperature goes up, achieving a maximum efficiency at a temperature of 350 °C of roughly 60%. Also, it was possible to verify that the pressure didn't affect significantly the performance of the MR system.

When it comes to the performance of the catalyst itself, it is possible to say, by the amount of CO_2 found in the retentate side of the membrane, that the CO is being converted into CO_2 and therefore the catalyst shows a good performance in the WGS reaction.

It is also worth mentioning that this system also produces almost no CH_4, which is a good result considering the fact this is one of the most important parameters to have into account when dealing with this kind of processes. Moreover, the Cu-based catalyst and other reaction species did not poison the membrane, being the value of permeation obtained from the permeation tests performed before and after the reaction test of the same order of magnitude (10^{-9} mol m^{-1} s^{-1} $Pa^{-0.5}$).

There was also the possibility to compare the results obtained during these experiments with other results gathered with different catalysts tested prior to this experiment at ENEA. The result is that, despite the better efficiency of the Pt-based on alumina support (CAT 2 - BASF) catalyst, this catalyst produced also too much CH_4 on the retentate side, when compared to the other two (CAT 1 and 3). Being CH_4 an undesired by-product, that catalyst shows to be unreliable when compared to the other two. It can be concluded that either the non-commercial (CAT 1 - Argentina) Pt-based with silica catalyst, or the commercial Cu based catalyst (CAT 3 – HiFuel ®) would be the best option in this aspect. Nevertheless, since the catalyst produced in Argentina is a catalyst that was made especially to be tested at ENEA and therefore there are high expenses in its manufacture/exportation since it is not commercialized, the Cu-based catalyst presented in this work may come up as a viable solution for the WSG reaction, not to mention that it shows better results in CO conversion into CO_2.

Even though these experiments were advantageous to have a general idea of how good the copper based catalyst from HiFuel ® was, investigation does not rely itself on only one set of experiments; for more reliable results it is necessary to repeat these tests and also, it would be interesting to check, in the future, what would happen in terms of efficiency and retentate gases composition when varying the CO/H_2O molar ratio with this new catalyst.

8 REFERENCES

Adhikari, S., & Fernando, S. (2006). *Hydrogen Membrane Separation Techniques* (Vol. 43). Mississippi, Mississippi, USA: Ind. Eng. Chem.

Cornaglia, C., Tosti, S., Sansovini, M., & Munera, J. (2013). Novel catalyst for the WGS reaction in a Pd-membrane reactori. *Applied Catalysis A: General, 462-463*, 278-286.

Freeman, B. D. (1999). *Basis of permeability/selectivity trade off relations in polymeric gas separation membranes* (Vol. 32). Raleigh, North Carolina, United States of America: Macromolecules.

Hatlevik, Ø. S. (2010). palladium and Palladium-alloy for hydrogen separation and production: History, fabrication strategies and current performance. *Separation and Purification technology, 73*(1), 59-64.

HO, W., & Sirkar, K. K. (1992). *Membrane Handbook.* New York: Chapman & Hall.

Hunter, J. B. (1956). *United States of America Brevetto n. US2773561 A.*

Johannesen, B. A. (2014, June). Microchannel Membrane Reactor for Production of pure Hydrogen. Troundheim, Norway.

K. S. Rothenberger, e. a. (2003). *, Evaluation of tantalum-based materials for hydrogen separation at elevated temperatures and pressures* (Vol. 218). Journal of membrane Science.

McLeod, L. S. (2008, December). Hydrogen Permeation Through Microfabricated Palladium-Silver Alloy Membranes . Giorgia, United States of America.

Miao, D., Cavusoglu, G., Henning , L., Jiafeng , Y., Hengyong , X., Jan-Dierk , G., & Andreas , G. (2017). Water-gas shift reaction over platinum/strontium apatite catalysts. In *Applied Catalysis B: Environmental:* (Vol. 202, p. 587-596).

Mulder, M. (1996). *Basic Principles of Membrane Techonology.* Kluwer Academic Publishers.

Nenoff, N. W. (2007). Membranes for Hydrogen Separation. In *Chem. Rev.* (p. 4078-4110).

Norby, T. (1999). Solid-state protonic conductors: principles, properties, progress and prospects,. *Solid State Ionics, 125*(1-4), 1-11.

Porter, A. B. (2000). A comparison of membrane separation and distillation. In *Chemical Engineering Research & Design 78* (p. 255).

Santucci, A. (2011/2012). PD-based Membrane Technology for Ultrapure Hydrogen Separation and Production. Roma: Università degli Studi di Roma - Facoltà di Ingegneria.

Santucci, A., Borgognoni, F., Vadrucci, M., & Tosti, S. (2013). Testing of dense Pd–Ag tubes: Effect of pressure and membrane thickness on the hydrogen permeability. *Journal of Membrane Science, 444*, 378-383.

Stern, S. A. (1991 - 1992). *Fundamentals of gas-Diffusion in rubbery and Glassy Polymers* (Vol. 423). New York, Siracuse, United States of America: ACS Symposium Series.

Tosti, S., Borgognoni, F., & Santucci, A. (2010). Electrical resistivity, strain and permeability of Pd-Ag membrane tubes. *International journal of hydrogen energy, 38*(10), 7796-7802.

Witjens, L. (2004). Synthesis and Characterisation of Pd/Ag Membranes for Hydrogen Separation. Rotterdam: Utrecht University.

Yun, S., & Oyama, S. T. (2011). Correlations in Palladium membranes for hydrogen separation: A review. *Journal of membrane science, 375*(1-2), 28-45.

9 APPENDIX

A. SIEVERTS' LAW GRAPHICS WITH FLUX OF HYDROGEN PERMEATED VS. DRIVING FORCE

The following figures allow to analyse if the results obtained in terms of flux as a function of the driving force follow Sieverts's law.

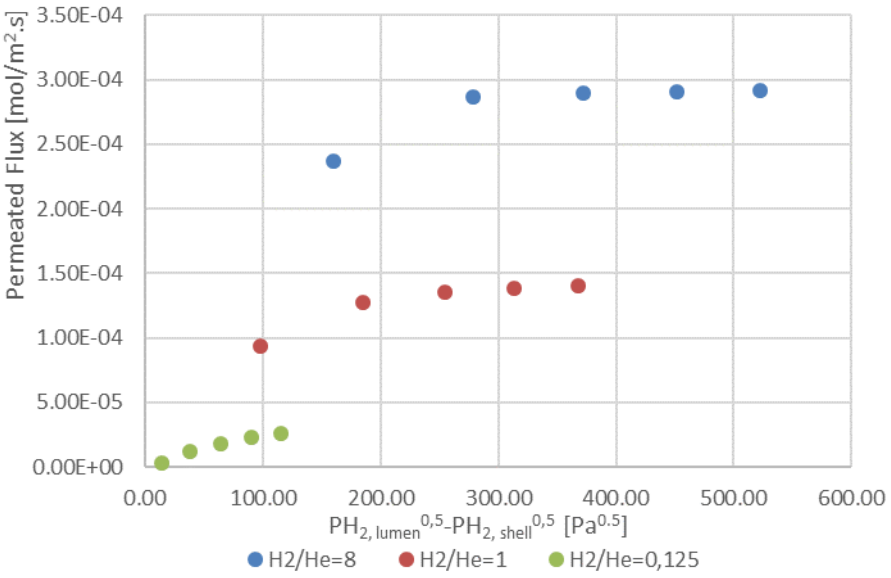

Figure 9.1 - Permeated flux of hydrogen [mol m^{-2} s^{-1}] as a function of the applied driving force [Pa$^{0.5}$] at a temperature of 400 °C

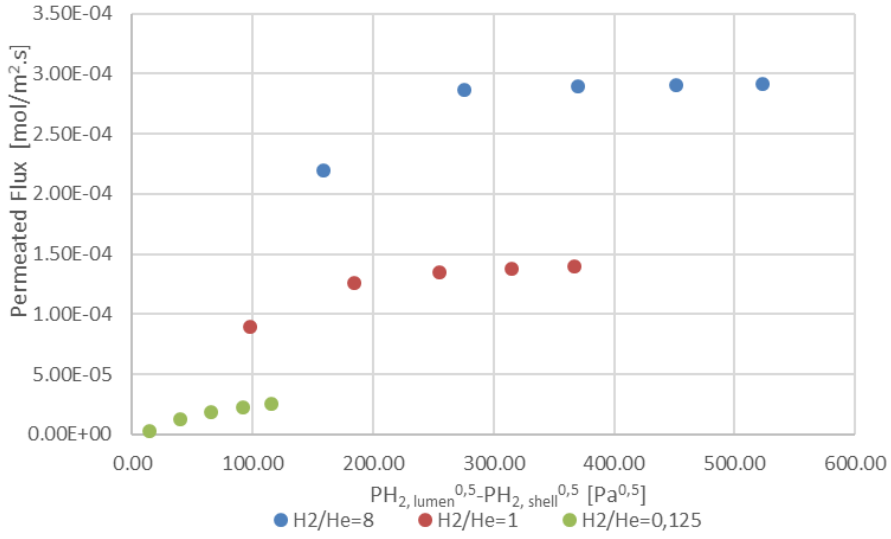

Figure 9.2 - Permeated flux of hydrogen [mol m^{-2} s^{-1}] as a function of the applied driving force [Pa$^{0.5}$] at a temperature of 350 °C

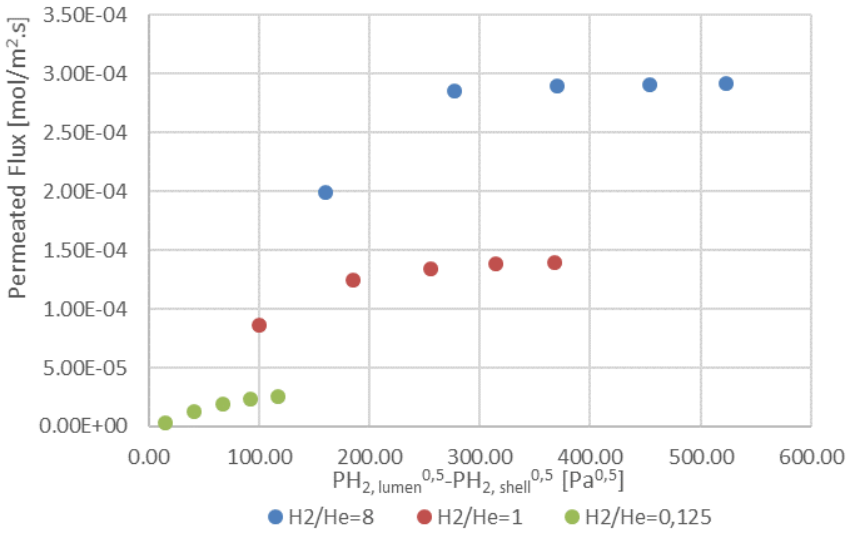

Figure 9.3 - Permeated flux of hydrogen [mol m^{-2} s^{-1}] as a function of the applied driving force [$Pa^{0.5}$] at a temperature of 300 °C

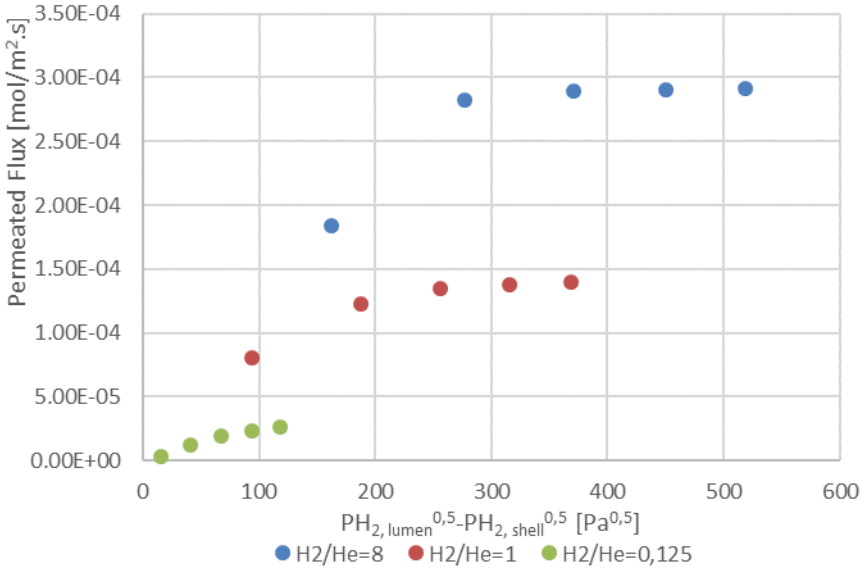

Figure 9.4 - Permeated flux of hydrogen [mol m-2 s-1] as a function of the applied driving force [$Pa^{0.5}$] at a temperature of 250 °C

Considering the figures presented above, it is possible to say the data does not fit the Sievert's law in all it is range. This fact is due to the recuperation of hydrogen being too high (>95%) and therefore the partial pressure of hydrogen is not the same in the whole extention of the tube. However, the Sievert's law can be proved by the data at lower total pressure where the recuperation of hydrogen is much lower.

B. Experimental Procedure of the Permeation and Reaction Tests

Starting procedure:

1) Start running and recording the acquisition and control program (Labview), adjusting the flow rate values of He desired and the acquisition time to 10 seconds;
2) After the He is flushing, switch on the heating system and the vacuum pumping system;
3) For the reaction test, start up the resistance to heat up the water;
4) When the membrane reaches the testing temperature, adjust the Hydrogen flow rate according to the conditions of the test to be executed (or CO and Water, if it is the reaction test);
5) Finally, adjust the pressure by closing or opening the valve.

Cool down procedure:

1) Lower the pressure by opening the valve;
2) Lower H_2/CO and water to zero sccm and raise He to 500 sccm;
3) Close the H_2/CO line and turn off all the heating;
4) When the membrane is at room temperature, start the leak test and turn off the vacuum pump.

Leak test procedure:

The leak test consists on the pressurization of the membrane with Helium at the end of the day and let the acquisition program running and recording data during the night.

1) Create a new file and start the acquisition program, changing the acquisition time to 1 minute instead of 10 seconds.
2) Increase pressure inside the membrane (usually until 3 bar);
3) Take the values of the temperature and pressure inside the membrane and compare the results in the morning to be sure there is no damage on the membrane.

Frequently, when the membrane was pressurized in the end of the day, the temperature of the membrane was still decreasing, which means the temperature inside the membrane will only be constant after two or three hours. For a better conclusion, it is necessary to take into the account the time elapsed between the two temperatures.

However, every morning the pressure difference between the beginning of the leak test and the end of the leak test was minimal, due to the decrease of the temperature during the night. So, after consideration, no leaking was considered at any point during the permeation test.

C. Calibration Curves used in the GC during the Reaction Tests

The calibration curves were calculated with the data taken directly from the software of the Gas Chromatographer according to calibration previously made by a specialized technician.

The data, at first, didn't fit the range of the calibration curve, therefore, there was needed to force all the curves to pass through zero. The same procedure was made by Marco Incelli in his results with the non-commercial catalyst (CAT 1) and the commercial catalyst BASF (CAT 2).

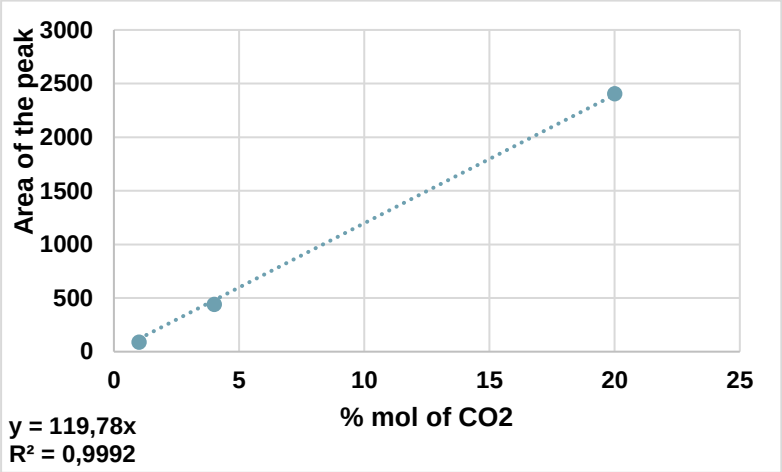

Figure 9.5 – Calibration Curve of the Gas Chromatograph for CO_2

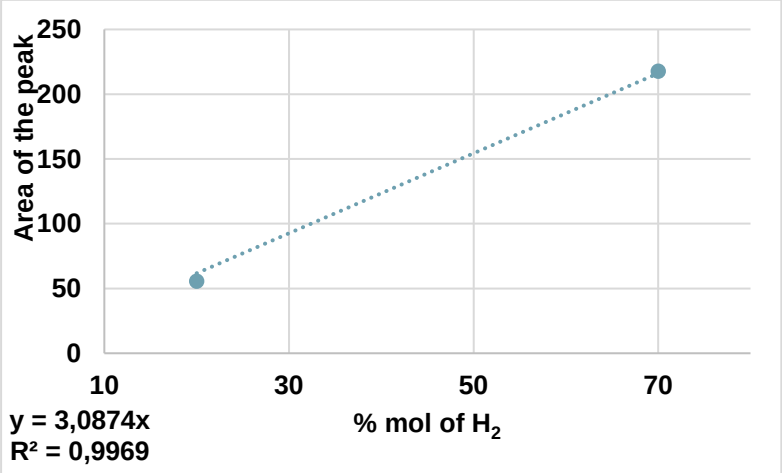

Figure 9.6 - Calibration Curve of the Gas Chromatograph for H_2

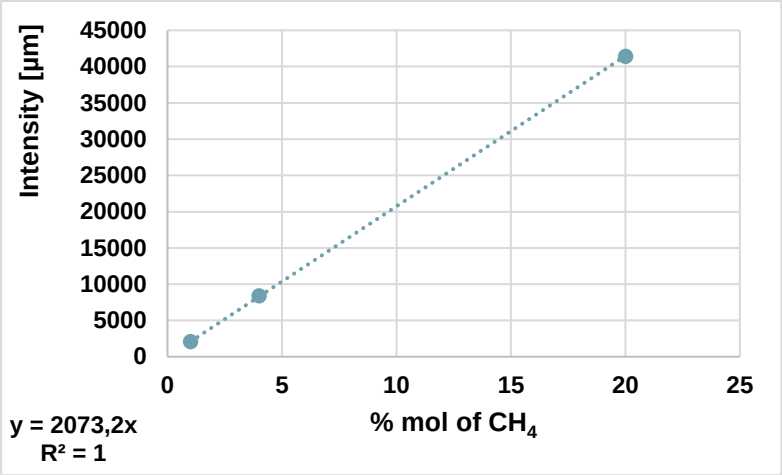

Figure 9.7 - Calibration Curve of the Gas Chromatograph for CH_4